

1 **Quality assessment of Second-generation Global Imager**
2 **(SGLI)-observed cloud properties using SKYNET surface**
3 **observation data**

4 Pradeep Khatri¹, Tadahiro Hayasaka¹, Hitoshi Irie², Husi Letu³, Takashi Y. Nakajima⁴, Hiroshi
5 Ishimoto⁵, and Tamio Takamura²

6
7 ¹Center for Atmospheric and Oceanic Studies, Graduate School of Science, Tohoku University, Sendai, Japan

8 ²Center for Environmental Remote Sensing, Chiba University, Chiba, Japan

9 ³Institute of Remote Sensing and Digital Earth, Chinese Academy of Sciences, Beijing, China

10 ⁴Research and Information Center (TRIC), Tokai University, Hiratsuka, Japan

11 ⁵Meteorological Research Institute, Tsukuba, Japan

12

13 *Correspondence to:* Pradeep Khatri (pradeep.khatri.a3@tohoku.ac.jp)

14

15 **Abstract.** The Second-generation Global Imager (SGLI) onboard the Global Change Observation Mission –
16 Climate (GCOM-C) satellite launched on December 23, 2017, observes various geophysical parameters with the
17 aim of a better understanding of the global climate system. As part of that aim, SGLI has great potential to unravel
18 several uncertainties related to clouds by providing new cloud products along with several other atmospheric
19 products related to cloud climatology, including aerosol products from polarization channels. However, a very
20 little is known about the quality of the SGLI cloud products. This study uses data about clouds and global
21 irradiances observed from the Earth’s surface using a sky radiometer and a pyranometer, respectively, to
22 understand the quality of the two most fundamental cloud properties—cloud optical depth (COD) and cloud-
23 particle effective radius (CER)—of both water and ice clouds. The SGLI-observed COD agrees well with values
24 observed from the surface, although it agrees better for water clouds than for ice clouds, while the SGLI-observed
25 CER exhibits poorer agreement than does the COD, with the SGLI values being generally higher than the sky
26 radiometer values. These comparisons between the SGLI and sky radiometer cloud properties are found to differ
27 for different cloud types of both the water and ice cloud phases and different solar and satellite viewing angles by
28 agreeing better for relatively uniform and flat cloud type and for relatively low solar zenith angle. Analyses of
29 SGLI-observed reflectance functions and values calculated by assuming plane-parallel cloud layers suggest that
30 SGLI-retrieved cloud properties can have biases on the solar and satellite viewing angles, similar to other satellite
31 sensors including the Moderate Resolution Imaging Spectroradiometer (MODIS). Furthermore, it is found that the
32 SGLI-observed cloud properties reproduce global irradiances quite satisfactorily for both water and ice clouds by
33 resembling several important features of the COD comparison, such as the better agreement for water clouds than

34 for ice clouds and the tendency to underestimate (resp. overestimate) the COD in SGLI observations for optically
35 thick (resp. thin) clouds.

36

37 **1. Introduction**

38 Clouds play important roles in changing the Earth’s climate system (Ramanathan et al., 1989), with profound
39 impacts on the atmospheric heat budget and the hydrological cycle (Rosenfeld et al., 2014). However, their strong
40 spatial and temporal variations as well as their complex interactions with aerosols and meteorology (e.g., Rosenfeld
41 et al., 2014; Khatri et al., 2020) have made it difficult to date to represent clouds accurately in global climate
42 models (Forster et al., 2021). Consequently, the roles of clouds in climate change are very poorly understood, and
43 they are highlighted as important sources of uncertainty in future climate projections (IPCC, 2021). Given their
44 importance, clouds are now being studied from different perspectives and using different methods, one of which
45 is cloud remote sensing from space, which has been in practice since the first successful capture of a cloud picture
46 by a Television InfraRed Observational Satellite (TIROS) launched on April 1, 1960. Since then, cloud remote-
47 sensing technology has advanced greatly, and there are currently several active and passive sensors onboard
48 various polar-orbiting or geostationary satellites to observe clouds from space. Because of their benefits of wide
49 spatial coverage and continuous observations at specific time intervals, satellite cloud products have been used
50 broadly either independently (e.g., Khatri et al., 2021) or combined with technologies such as numerical simulation
51 or artificial intelligence (e.g., Masunaga et al., 2008; Letu et al., 2020, 2021), for a better understanding of cloud
52 climatology as well as energy and water budgets. However, because the same satellite sensor monitors either the
53 whole Earth or a large part of it for a long time and the cloud products are generally generated by processing
54 satellite-received signals using certain physical models and assumptions (e.g., daytime cloud optical depth (COD)
55 and cloud-particle effective radius (CER) are obtained using the reflectance observed at two different wavelengths
56 by assuming clouds to be plane-parallel horizontal (PPH) layers), assessing the quality of such cloud products is a
57 fundamental requirement for using them in scientific research, policy making, and other application areas.
58 Furthermore, such quality-assessment studies help in gathering important information that is useful for developing
59 next-generation satellite sensors and observation techniques that overcome the shortcomings of existing
60 technologies.

61 The Global Change Observation Mission – Climate (GCOM-C) satellite (or “Shikisai” in Japanese) is a polar-
62 orbiting satellite that was launched on December 23, 2017. Onboard is the Second-generation Global Imager
63 (SGLI), which has 16 channels covering the spectrum from ultraviolet to thermal infrared. Of these 16 channels,
64 the 1.05-, 1.63-, and 2.21- μm channels in the shortwave infrared region and the 10.8- μm channel in the thermal
65 region are used to infer the properties of both water and ice clouds (Nakajima et al., 2019). Having entered
66 operation relatively recently, very little is known about the quality of the cloud products generated from the SGLI
67 satellite sensor, thereby emphasizing the need and urgency for assessing the quality of SGLI cloud products. In
68 addition, SGLI is a powerful sensor for observing aerosols because of the inclusion of polarization and
69 bidirectional channels, thereby making it very useful for studying aerosol–cloud interaction with qualitative

70 aerosol data. Therefore, studies related to assessing the quality of SGLI cloud products can also contribute to
71 aerosol–cloud interaction studies performed using SGLI data.

72 A literature review shows the scarcity of quality-assessment studies for SGLI cloud products. Nakajima et al.
73 (2019) performed such a study by comparing SGLI cloud products with those obtained from the Moderate
74 Resolution Imaging Spectroradiometer (MODIS) sensor onboard the Terra satellite; they found very good
75 agreement between the MODIS and SGLI cloud products for both water and ice clouds over both ocean and land
76 surfaces. Because cloud retrievals from MODIS and SGLI are based on the same retrieval framework of Nakajima
77 and King (1990) and similar types of cloud reflectance data, it is very important to assess the quality of SGLI cloud
78 products by using data of different natures obtained from different observation techniques, such as those obtained
79 from surface observations. Damiani et al. (2019) compared SGLI-observed COD with surface-observed values
80 obtained using different instruments, including a sky radiometer and a pyranometer; they found reasonably good
81 agreement between the SGLI and surface observations, but their study was limited to an observation period of a
82 few days (16 days) with very few samples for comparison and for water cloud COD only. By contrast, the present
83 study is designed to use long-term observation data from multiple sites to assess the quality of the properties of
84 both water and ice clouds.

85 This paper is organized as follows. Sections 2 and 3 describe the data and the study method, respectively.
86 Section 4 presents and discusses the results. Finally, section 5 summarizes the main findings of this study.

87

88 **2. Data**

89 **2.1. SKYNET**

90 Data from SKYNET sites in Japan (Table 1) for 2018–2020 were used in the present study. These sites have
91 different atmospheric backgrounds: Chiba and Sendai are urban sites, whereas Hedo-misaki, Fukue-jima, and
92 Miyako-jima are located on the coast of the east China Sea, where a different air mass—either marine or long-
93 range transported continental—prevails in different seasons (Khatri et al., 2010, 2014a), making them unique for
94 studying aerosols and clouds. Except for Sendai, all these sites are “super sites” of SKYNET, being equipped with
95 various instruments for observing aerosols, clouds, radiation, and meteorology. We used two types of SKYNET
96 data as described below.

97

98 **2.1.1. Sky radiometer**

99 Nakajima et al. (2020) described in detail the sky radiometer technology of SKYNET. Although sky radiometer
100 data have been used widely to study aerosol properties (e.g., Hashimoto et al., 2012; Wang et al., 2014; Khatri
101 et al., 2016; Mok et al., 2018; Irie et al., 2019), retrievals of ozone (Khatri et al., 2014b), water vapor (Campanelli
102 et al., 2014), and clouds (Khatri et al., 2019) are also possible from sky radiometer observations. The present study
103 used cloud properties retrieved from a sky radiometer (POM-02; PREDE Co., Ltd., Japan) that observed spectral
104 zenith radiances at 10-min intervals. Of 11 wavelengths between ultraviolet and near-infrared, the zenith radiances
105 observed at 0.87, 1.02, and 1.627 μm were used to obtain COD and CER via a cloud retrieval algorithm by Khatri
106 et al. (2019). Aerosol observations made at the wavelengths of 0.38, 0.4, 0.5, 0.675, 0.87, and 1.02 μm under clear

107 sky conditions were used to derive the temporal (monthly) variations of the calibration constants for the
108 wavelengths of 1.627 μm (absorbing) and 0.87 μm and 1.02 μm (non-absorbing) to convert the observed signals
109 into transmittances. These spectral transmittances were then combined with spectral surface reflectance and
110 precipitable water content (PWC) to retrieve COD and CER simultaneously via an optimal method (Rodgers,
111 2000). The surface reflectance and PWC data were obtained from MODIS and Modern-Era Retrospective Analysis
112 for Research and Applications, Version 2 (MERRA-2), respectively. In retrieving the properties of water clouds,
113 single-scattering properties generated for spherical water cloud droplets estimated from Mie calculations were
114 used, whereas such databases corresponding to the Voronoi model of irregular shapes for ice particles (Ishimoto
115 et al., 2012) were used in retrieving the properties of ice clouds.

116

117 **2.1.2. Pyranometer**

118 Each SKYNET site in Japan is equipped with a pyranometer (Kipp and Zonen, Holland) to measure
119 downwelling global irradiances. Because the global irradiance over Miyako-jima was observed for only a limited
120 study period, the data from the remaining four sites were used in this study. The observed global irradiances were
121 for the spectral range of 0.315–2.8 μm and for a temporal resolutions of 60 s for Sendai and 20 s for the other sites.

122

123 **2.2. SGLI**

124 We used the Level 2.0 (Version 2.0) cloud products of SGLI (Nakajima et al., 2019). The GCOM-C satellite
125 carrying the SGLI sensor is timed to cross the equator from north to south at approximately 10:30 AM local time,
126 and the spatial resolution of the SGLI cloud product is 1 km \times 1 km at nadir. The SGLI cloud products were
127 retrieved using the CAPCOM cloud property retrieval algorithm (Nakajima and Nakajima, 1995; Kawamoto et al.,
128 2001; Nakajima et al., 2019), in which the 1.05- and 2.21- μm channels were used as the non-absorbing and
129 absorbing wavelengths, respectively, while developing the look-up table (LUT) of cloud reflectance (Nakajima
130 and King, 1990). The LUTs for water clouds and ice clouds were developed using the single-scattering properties
131 of spherical water cloud droplets calculated using Mie theory and non-spherical Voronoi particles (Ishimoto et al.,
132 2012). Along with those reflectance data, the algorithm also used ancillary data such as vertical profiles of
133 temperature, water vapor, and surface reflectance while retrieving cloud properties (Nakajima et al., 2019).

134

135 **3. Study method**

136 Depending on the departure of the viewing angle of the satellite sensor from nadir, a parallax—that is, a shift
137 in cloud position (longitude and latitude) from that corresponding to the surface—can occur, and correcting this
138 parallax is important when comparing oblique-view satellite products with observations made either at nadir view
139 from space (e.g., Khatri et al., 2018a) or at zenith view from the surface (e.g., Khatri et al., 2018b). Therefore, the
140 SGLI cloud products were parallax-corrected by using information about cloud-top height, the zenith and azimuth
141 angles of the satellite, and the position (latitude and longitude) of the observation site. Then, if all satellite pixels
142 with 5 \times 5 coverage and the observation site at the central pixel were cloudy, they were used to calculate the
143 average values of COD and CER. They were then compared with the sky radiometer values observed at the surface

144 within ± 30 min of the SGLI observation time. Such averaging practices can address cloud movement (Cess et al.,
 145 1996) and are common in validating satellite cloud products using surface observation data. For example, Dong
 146 et al. (2008) and Yan et al. (2015) compared CERES-MODIS cloud properties averaged over a $30 \text{ km} \times 30 \text{ km}$
 147 square and a circle of 20-km radius around the observation site, respectively, with surface observation values
 148 averaged over a 1-h period.

149 The pyranometer-observed global irradiances were further used to assess the quality of the SGLI cloud products.
 150 For this purpose, the SGLI cloud properties and ancillary data such as PWC from MERRA-2 and spectral surface
 151 reflectance from MODIS were used in an RSTAR radiative-transfer model (Nakajima and Tanaka, 1986, 1988) to
 152 calculate downwelling global irradiances in the $0.315\text{--}2.8\text{-}\mu\text{m}$ spectral range. The single-scattering properties
 153 obtained from Mie calculations for water clouds and those corresponding to the Voronoi model for ice clouds were
 154 used for water and ice clouds, respectively. The modeled global irradiances of the 5×5 pixels centered on the
 155 observation site were then averaged to compare with the values observed at the surface for ± 5 min centered on the
 156 SGLI observation time.

157 To quantify the degree of agreement between the SGLI and surface observations, the mean bias error (MBE),
 158 root-mean-square error (RMSE), and correlation coefficient (r) values were calculated as

$$159 \quad MBE = \frac{1}{n} \sum_{i=1}^n (G_i - S_i), \quad (1)$$

$$160 \quad RMSE = \sqrt{\sum_{i=1}^n \frac{(G_i - S_i)^2}{n}}, \quad (2)$$

$$161 \quad r = \frac{n(\sum_{i=1}^n G_i S_i) - \sum_{i=1}^n G_i \sum_{i=1}^n S_i}{\sqrt{[n \sum_{i=1}^n G_i^2 - (\sum_{i=1}^n G_i)^2][n \sum_{i=1}^n S_i^2 - (\sum_{i=1}^n S_i)^2]}}, \quad (3)$$

162 where G_i and S_i are surface and satellite observations, respectively, and n is the total sample count.

163

164 4. Results and discussion

165 4.1. Comparison between SGLI-observed and sky radiometer-observed cloud properties

166 4.1.1. Overall comparison

167 The COD values from the sky radiometer and SGLI are compared in Figure 1(a) and (b) for water clouds and
 168 ice clouds, respectively. In general, the values from the two different sources agree reasonably well for both cloud
 169 types. The r value for water clouds is higher than that for ice clouds, suggesting that the temporal variations of
 170 COD from the sky radiometer and SGLI are more consistent with each other for water clouds than for ice clouds.
 171 The MBE values are positive and nearly the same for water and ice clouds. Overall, these positive MBE values
 172 suggest smaller COD from SGLI than from the sky radiometer for both water and ice clouds, but upon closer
 173 inspection, Figure 1 indicates that whether the COD from SGLI is an overestimate or an underestimate depends
 174 on the COD value; we have underestimated values from SGLI for relatively high COD for both water and ice
 175 clouds, whereas most of the data samples show an overestimated COD from SGLI when they are less than ~ 20
 176 and ~ 10 for water and ice clouds, respectively. A literature review also suggests similar results in the past for COD
 177 observed by other remote-sensing tools. For example, King et al. (2013) and Liu et al. (2013) showed
 178 overestimated (resp. underestimated) COD for values less (resp. greater) than ~ 20 when they compared MODIS

179 COD with values obtained from in situ aircraft observations and a multifilter rotating shadowband radiometer,
180 respectively. Nakajima et al. (1991) also found overestimation (resp. underestimation) of COD for values less
181 (resp. greater) than ~ 10 while comparing their products retrieved from cloud reflection measurements with those
182 obtained from in situ aircraft observations. Khatri et al. (2018b) also found similar results when they compared
183 COD values observed by MODIS and the Advanced Himawari Imager with surface-observed values. The
184 consistency of Figure 1 with those previous studies indicates that reflectance-based COD from satellite retrieved
185 by assuming PPH cloud layers (i.e., by using one-dimensional (1D) radiative transfer theory) can be
186 underestimated (resp. overestimated) for optically thin (resp. thick) clouds irrespective of sensor type. It can be
187 noted in a Nakajima-King diagram that COD increases (decreases) with the decrease (increase) of value
188 corresponding to absorbing wavelength even without any change of value corresponding to non-absorbing
189 wavelength. Since satellite-observed signal corresponding to absorbing wavelength is mostly from upper portions
190 of clouds, it can be less than the value that can result from whole cloud layers. Under such condition, retrieved
191 COD can be overestimated. However, subpixel inhomogeneity is commonly known to underestimate retrieved
192 COD in satellite observation when clouds are assumed to be PPH layers (Cahalan et al., 1994). Cahalan et al.
193 (1994) suggested that such subpixel inhomogeneity effect, which is also called as "plane-parallel albedo bias", is
194 very weak for thin clouds and very thick clouds reaching albedo saturation, but strong for moderately thick clouds.
195 Thus, these two different effects may counter each other to increase or decrease COD. The less influence of "plane-
196 parallel albedo bias" for thin clouds may result SGLI-observed CODs higher than sky radiometer-observed values
197 for relatively thin clouds. On the other hand, the opposite for relatively thick clouds could be the result of dominant
198 effect of "plane-parallel albedo bias". A detailed investigation is required in the future to further clarify the
199 mechanism for such results.

200 The CER values from the sky radiometer and SGLI are compared in Figure 2 (a) and (b) for water clouds and
201 ice clouds, respectively. The CER values show poorer agreement than do the COD values in the comparisons for
202 both water and ice clouds. There can be a number of reasons for such poorer agreement for CER. First, unlike
203 surface-based sky radiometer, the upper portions of clouds are sampled more readily than lower parts in space-
204 based SGLI. Since cloud-droplets can have vertical inhomogeneity with upper cloud portions containing both
205 relatively large-sized (e.g., an adiabatic growth at the beginning of cloud generation) as well as small-sized (e.g.,
206 entrainment of dry air at the cloud top, collision-coalescence process) particles, CERs retrieved from SGLI
207 observations can become both larger and smaller than those retrieved from sky radiometer observations, as noted
208 in Figure 2, depending on vertical inhomogeneity of clouds. Further, as the absorbing wavelengths, which are
209 critical for CER retrievals, corresponding to current SGLI and sky radiometer cloud retrieval algorithms are 2.2
210 and 1.6 μm , respectively, these different wavelengths can have different absorptions to further enhance the
211 difference in CER between SGLI and sky radiometer. Except them, quality of data samples used for the comparison
212 holds an important position to determine the comparison metrics, such as r value, RMSE, and MBE. For example,
213 if we screen data shown in Figures 1 and 2 by selecting only those that have coefficient of variation (COV), i.e.,
214 the ratio of standard deviation value to the mean value, less than 0.2 for CODs of both sky radiometer and SGLI,
215 the comparison metrics, including those for CER comparisons, can have different values (Figure 3). CODs with

216 COV less than 0.2 for sky radiometer (SGLI) can represent data samples having very less temporal (spatial)
217 variations in sky radiometer (SGLI) observations, indicating relatively strict data screening criteria for comparison.
218 Figure 3(a) shows a very good agreement for CER comparison for water clouds. On the other hand, the comparison
219 metrics corresponding to CER comparison for ice clouds are still poor because a limited number of samples show
220 considerably large difference between sky radiometer and SGLI. However, on the other side, it is still encouraging
221 to see a considerable number of samples falling around 1:1 line in Figure 3(b). Nevertheless, Figure 3 suggests an
222 important role of data handling procedure while evaluating cloud properties obtained from space-based
223 observations with those from surface-based observations. Further, as the number of scattering within cloud layers
224 increases with the increase of cloud thickness, COD can be suggested to play an important role in retrieved CER
225 value. The influence of COD on retrieved CER in satellite remote sensing has been discussed in detail from both
226 theoretical (e.g., Nakajima and King, 1990) as well as observation perspectives (e.g., Zhang and Platnick, 2011).
227 Similarly, Khatri et al. (2019) showed the influence of COD on retrieved CER for surface-based sky radiometer.
228 Figure 4 shows the relationship between CER difference, i.e., ΔCER ($\text{CER}_{\text{SGLI}} - \text{CER}_{\text{skyrad}}$) and COD_{SGLI} for water
229 clouds and ice clouds. In general, Figure 4 suggests a negative correlation between ΔCER and COD_{SGLI} . Such
230 negative correlation is relatively less prominent for ice clouds than for water clouds, which can probably due to
231 irregular shapes of ice cloud particles that adds complexity while retrieving cloud properties in both sky radiometer
232 and SGLI observations. Figure 4(a) suggests that SGLI and sky radiometer CERs, in general, may have relatively
233 close agreement for CODs around 20. Note that CODs from SGLI and sky radiometer also show relatively close
234 agreement for CODs around 20, as discussed above. Figure 4(a) further suggests that CER values from SGLI can
235 be higher (lower) than sky radiometer values when clouds are relatively thin (thick). This result again coincides
236 with relatively higher values of COD from SGLI than those from sky radiometer for relatively thin (thick) clouds.
237 On the other hand, Figure 4(b) suggests that relatively very large difference in CER between SGLI and sky
238 radiometer can generally occur for relatively thin clouds. Note that retrieved CERs can have larger uncertainties
239 for optically thinner clouds in both surface and satellite retrievals (Khatri et al., 2019; Nakajima and King, 1990).
240 Nevertheless, Figure 4 suggests that CER difference between SGLI and sky radiometer can vary differently
241 depending on COD value, suggesting COD as one important candidate for CER difference between them. Along
242 with these factors, differences in ancillary and surface reflectance data in the retrieval algorithms of SGLI and sky
243 radiometer may also contribute partially to bring differences in retrieved values of CER as well as COD between
244 SGLI and sky radiometer. Although such manifold factors can be responsible for differences in CER values
245 between SGLI and sky radiometer, most of the data samples show higher CER values from SGLI than from the
246 sky radiometer, resulting in negative values of MBE for both water and ice clouds. This result is in line with
247 previous studies that showed higher values from satellite observations compared with values obtained from surface
248 and/or aircraft observations (e.g., Painemal and Zuidema, 2011; Chiu et al., 2012; King et al., 2013).

249 The comparison results discussed above suggest some future research scopes. Since cloud-droplet vertical
250 inhomogeneity can have important effects on retrieved cloud properties for both space- and surface-observation
251 data, future studies may effectively implement observation data of active sensors, such as surface-observation
252 based lidar, as well to improve and strengthen the quality assessment of CER values obtained from SGLI and other

253 similar satellite sensors. Furthermore, CER retrievals from SGLI (sky radiometer) may be extended for absorbing
254 wavelength of 1.6 μm (2.2 μm) for further improving and strengthening such quality assessment studies as well as
255 expanding our understanding regarding CER property. In addition, along with sky radiometer, other surface-based
256 radiometers, such as rotating shadow-band spectro-radiometer (Khatri et al., 2012; Takamura and Khatri, 2021),
257 that have wide field of view (FOV) can be brought in use for remote sensing of cloud properties from surface and
258 to validate space-observed cloud properties more rigorously.

259

260 **4.1.2. Comparison by separate cloud type**

261 The SGLI cloud product also contains information about cloud type, which is determined based on COD and
262 cloud top pressure (CTP), similar to the cloud classification method of the International Satellite Cloud
263 Climatology Project. The data for water clouds shown in Figures 1(a) and 2(a) correspond to the altostratus,
264 nimbostratus, stratocumulus, and stratus cloud types. Figure 5 compares the sky radiometer and SGLI cloud
265 properties for each cloud type. Since comparison between SGLI and sky radiometer is performed for spatial and
266 temporal averages of SGLI and sky radiometer observations, respectively, the cloud type used in this study
267 corresponds to the pixel located at the center of 5x5 SGLI pixels, which includes observation site. Of these four
268 types of clouds, the first two are mid-level clouds and the last two are low-level clouds, which have CTP value of
269 440–680 hPa and greater than 680 hPa, respectively. Similarly, altostratus and stratocumulus have COD values of
270 3.6–23, but nimbostratus and stratus have COD values greater than 23. In Figure 5, stratus clouds show the best
271 agreement; compared to the other types of clouds, stratus clouds are more uniform and flatter, thereby being the
272 closest to PPH cloud layers. After stratus clouds, nimbostratus clouds suggest the next-best agreement, although
273 some CER values show large deviations from the 1:1 line. Because nimbostratus is a thick mid-level cloud, ice
274 crystals or their combination with liquid cloud droplets—including supercooled droplets—can form in and around
275 the cloud top, although middle and lower cloud portions can contain water cloud droplets. Under such conditions,
276 retrievals from SGLI by considering the cloud phase as being water can affect the retrieved products significantly,
277 especially CER, which in turn can cause considerably large differences from the CER observed from the surface.
278 To some extent, the results from the sky radiometer can also be affected. But, since the sky radiometer observes
279 from the surface, the dominant fractions of water in the middle and lower parts of such clouds have important
280 influences on surface-observed radiances, which may make considering the water cloud phase reasonably valid in
281 retrieval of cloud properties from surface observations for such conditions. On the other hand, altostratus and
282 stratocumulus clouds show moderate agreement for COD but poor agreement for CER. Because these clouds can
283 have COD values ranging from 3.6 to 23, large differences in CER comparison can arise, especially for relatively
284 thin clouds. This is because the uncertainties in CER retrievals can be larger for thin clouds than for thick clouds
285 in both sky radiometer and SGLI retrievals. Additionally, the high-level altostratus cloud can comprise ice and/or
286 supercooled droplets near the cloud top to affect SGLI retrievals, as discussed above. Regarding low-level
287 stratocumulus clouds, they may not contain such ice and/or supercooled liquid particles, but their cloud tops can
288 be quite inhomogeneous because they are generally clumps of thick and thin clouds, resulting in a higher degree
289 of cloud heterogeneity, which in turn can have large effects on satellite retrievals, as revealed from both modeling

290 (e.g., Iwabuchi and Hayasaka, 2002) and observation (e.g., Várnai and Marshak, 2007). Because SGLI has a larger
291 FOV than does the sky radiometer, instrumental FOV could be the next important factor for the large difference
292 between the sky radiometer and SGLI results for such highly heterogenous stratocumulus clouds.

293 Figure 6 compares the sky radiometer-observed and SGLI-observed cloud properties for different types of ice
294 clouds. As shown, seven types of ice phase clouds were detected, of which cirrus, cirrostratus, and deep convective
295 are high-level clouds, altocumulus, altostratus, and nimbostratus are mid-level clouds, and stratocumulus is a low-
296 level cloud. Cirrus and altostratus clouds have COD values of less than 3.6. These thin clouds have values of both
297 COD and CER that deviate largely from the 1:1 line, suggesting that large differences between the sky radiometer
298 and SGLI results can occur for thin clouds. This is because retrievals become ambiguous, resulting in two possible
299 solutions in both satellite retrieval (Nakajima and King, 1990) and sky radiometer retrieval (Khatri et al., 2019)
300 for such thin clouds. Furthermore, the sky radiometer-observed values are averages of ± 30 min centered on the
301 SGLI overpass time, making it possible to include some nearby thick clouds not included in the 5×5 pixels of
302 SGLI observation, given that the wind speed can be high at high altitudes. Cirrostratus followed by altostratus
303 occupy significant numbers of the ice cloud data. Furthermore, these cloud types agree better than do the other
304 types; they are generally uniform stratiform (layered) genus-type, that is, closer to PPH cloud layers than are the
305 other types of clouds. However, despite having the best agreement, some considerably large differences between
306 the sky radiometer and SGLI results still exist; these could be due to high wind speed, especially for cirrostratus,
307 a mixture of both water and ice cloud droplets, especially for altostratus, and the irregular shapes of ice crystals.
308 Deep convective and nimbostratus clouds have COD values of greater than 23. Although the top layers of these
309 clouds generally contain irregularly shaped ice crystals, their middle and lower parts can contain water cloud
310 droplets and/or supercooled droplets, making it difficult to retrieve cloud properties from both SGLI and the sky
311 radiometer by using a database of a single type of cloud phase. These thick clouds suggest fairly good agreement
312 between the sky radiometer and SGLI cloud properties, as do the low-level stratocumulus clouds detected as ice
313 clouds by SGLI. Note that there appears a data sample with mean COD for SGLI less than 23 in Fig. 6(c). Though
314 ISCCP defines deep convective cloud with COD greater than 23, the anvil portion of deep convective clouds can
315 have COD less than 23. Thus, a part of cloud pixels around the central pixel is likely to be anvil cloud to result
316 mean COD less than 23 for that case. Overall, the above comparison results for different types of clouds for both
317 water and ice phases reveal that cloud properties retrieved from the sky radiometer and SGLI can agree better if
318 the clouds are relatively uniform, flat, and thick.

319

320 **4.1.3. Effects of solar and satellite viewing geometries on comparison results**

321 Satellite cloud products retrieved by assuming PPH cloud layers can have biases depending on solar zenith
322 angle (SZA) (Kato and Marshak, 2009) and satellite viewing zenith angle (VZA) (Várnai and Marshak, 2007). To
323 understand how such SZA and VZA biases might influence the differences between SGLI and sky radiometer
324 cloud properties, comparisons are performed by separating the data for each SZA and VZA greater than and less
325 than 30° . The comparison results corresponding to water and ice clouds are shown in Figures 7 and 8, respectively.
326 Note that the SZA and VZA values used in this study correspond to the pixel located at the center of 5×5 SGLI

327 pixels. To understand further how SZA and VZA biases might influence the comparison results, we calculated the
 328 mean values of SZA and VZA for different levels of agreement in the sky radiometer and SGLI comparisons. In
 329 other words, these mean values were calculated by identifying very good agreement (difference less than 30%),
 330 moderate agreement (difference within 30%–60%), poor agreement (difference within 60%–90%), and very poor
 331 agreement (difference greater than 90%), where the difference is $|x_{SGLI} - x_{sky}|/x_{sky} \times 100\%$ and x represents
 332 COD or CER. The mean values are summarized in Tables 2 and 3 for water and ice clouds, respectively. Figures 7
 333 and 8 both show better agreements between the sky radiometer and SGLI COD values for $SZA < 30^\circ$ than for SZA
 334 $> 30^\circ$. Also, Table 2 suggests that increasing SZA increases the COD difference for water clouds. Although not
 335 distinct as in the case of water clouds, the COD difference for ice clouds also indicates its dependency on SZA in
 336 Table 3. These results suggest possible SZA bias in SGLI-observed COD and so its influence on the COD
 337 differences between the sky radiometer and SGLI. Both observations (e.g., Loeb and Davies, 1997) and radiative-
 338 transfer model simulations (e.g., Kato et al., 2006) suggest that COD retrieved by assuming PPH cloud layers
 339 increases with SZA because the horizontal leakage of radiation from cloud sides decreases relative to overhead
 340 Sun (Fu et al., 2000) and cloud sides have a greater opportunity to intercept more solar radiation for oblique Sun
 341 to increase the cloud-top-leaving radiance (Loeb et al., 1997). On the other hand, there appears to be no clear
 342 improvement in COD comparison between the sky radiometer and SGLI with increasing or decreasing VZA.
 343 However, as revealed from Figure 7, the COD comparison between the sky radiometer and SGLI for water clouds
 344 may deteriorate considerably when both SZA and VZA become large. Supporting this result, Table 2 shows higher
 345 values of VZA for cases of moderate and poor agreement than for very good and moderate agreement for water
 346 clouds. However, there seems to be no clear signature of the dependence of COD difference on VZA for ice clouds
 347 in Table 3. Liang and Di Girolamo (2013) suggested that satellite COD retrieved under the assumption of PPH
 348 cloud layers can either decrease or increase with VZA depending on the competition among multiple factors
 349 governed by SZA, relative azimuth angle (RAZ), and cloud inhomogeneity. This can plausibly explain the unclear
 350 effects of VZA on the COD comparisons shown in Figures 7 and 8 and summarized in Tables 2 and 3. For CER,
 351 it is almost impossible to say how SZA and VZA influence the CER comparisons shown in Figures 7 and 8,
 352 although to some extent it is likely that water clouds exhibit better agreement for low SZA than for high SZA.
 353 Coinciding with the results shown in Figures 7 and 8, Tables 2 and 3 also discard the influences of SZA and VZA
 354 on the CER differences between the sky radiometer and SGLI. Because the cloud properties observed from SGLI
 355 and the sky radiometer depend strongly on cloud type, as discussed above, and CER retrievals have larger
 356 uncertainties than do COD retrievals, these factors possibly diluted the influences of SZA and VZA on the CER
 357 differences between the sky radiometer and SGLI.

358 SZA and VZA biases on retrieved cloud properties for other satellite sensors—including MODIS—have been
 359 studied widely, but such studies for the SGLI sensor have been lacking to date. We further analyzed the SGLI
 360 observed reflectance (R) to shed further light on possible biases on the SGLI-retrieved cloud properties. For this
 361 purpose, the SGLI-observed R ($1.05 \mu\text{m}$) data with values of less than 1 for 500 pixels centered on the Chiba
 362 observation site were analyzed. Those data correspond to 2020. R values corresponding to different values of COD
 363 ($\text{COD} = 2\pm 1, 4\pm 1, 8\pm 1, 16\pm 1, 32\pm 1, 64\pm 1$) and SZA ($SZA = 20^\circ\pm 1^\circ\text{--}60^\circ\pm 1^\circ$ in 5° intervals) were binned by

364 accounting for the relative azimuth angle (RAZ), that is, the difference in azimuth angles between Sun and satellite.
365 Figure 9 shows the R -VZA relationships for these values of COD and SZA. Negative (resp. positive) VZA
366 corresponds to RAZ greater (resp. less) than 90° , representing forward (resp. backward) scattering. Because the
367 R -VZA relationship is similar for ice clouds, it is not shown here. The data fluctuations in Figure 9 for the same
368 values of COD and SZA suggest variations of CER and surface and atmospheric conditions. To tally such observed
369 R -VZA relationships, we again calculated R ($1.05 \mu\text{m}$) for the COD values of 2, 4, 8, 16, 32, and 64 with a fixed
370 CER of $8 \mu\text{m}$ and SZA values of 20° – 60° with intervals of 5° by assuming PPH cloud layers (Figure 10). These
371 calculations were performed for RAZ values of 135° and 45° to understand the characteristics of forward and
372 backward scattering, respectively. The calculated results shown in Figure 10 reveal that the R -VZA relationship
373 for ideal PPH cloud layers can have different shapes depending on SZA. For low SZA, the differences in R between
374 the forward and backward scattering directions are relatively small, increasing gradually with increasing SZA; for
375 high values of SZA, the R values in the forward scattering directions are higher than those in the backward
376 scattering direction. The shapes of the R -VZA relationship for ideal PPH cloud layers, which correspond to the
377 LUT databases of satellite retrieval algorithms, are different than those shown in Figure 9 corresponding to actual
378 observations, suggesting that three-dimensional (3D) cloud effects on observed signals are not captured well in
379 1D radiative-transfer calculations. Liang and Girolamo (2013) suggested that the observed VZA dependence of
380 COD (or R) is the weighted sum of different competing factors associated with Sun and satellite positions and
381 cloud inhomogeneity. For example, Várnai and Marsak (2007) found increased values of COD with increasing
382 VZA in both the forward and backward scattering directions, and they suggested that the dark gaps between cloud
383 fields could be filled up by brighter cloud sides through photon leakage when partly cloudy scenes are viewed
384 more obliquely, leading to higher values of COD in both the forward and backward scattering directions. On the
385 other hand, Loeb and Coakley (1998) found decreased and increased COD in the forward and backward scattering
386 directions, respectively, which they attributed to shadowing and illumination. Nevertheless, the most important
387 information revealed from Figures 9 and 10 is that 1D radiative-transfer theory may hardly capture the features of
388 R observed by SGLI, suggesting SZA and VZA biases on the retrieved cloud properties from SGLI, similar to
389 other satellite sensors including MODIS.

390

391 **4.2. Comparison between modeled and observed global irradiances**

392 Because surface-observed global irradiances vary strongly with cloud variation (Khatri and Takamura, 2009;
393 Damiani et al., 2018), they can also help to justify the comparison results discussed above. Specifically, surface-
394 observed global irradiances can be effective for evaluating satellite-observed COD values because the variation of
395 COD is more dominant than the variation of CER in the variation of global irradiance (Khatri et al., 2018b).
396 Figure 11 compares the measured and modeled global irradiances at the four observation sites that have
397 observation data for the whole study period for water clouds (Figure 11(a)) and ice clouds (Figure 11(b)). These
398 comparisons are for the mean values of the 5×5 SGLI pixels and ± 5 min of surface observations centered on the
399 SGLI observation time. The measured global irradiances agree very well with the observed values for both water
400 clouds and ice clouds. In both cases, the correlations are very strong with values greater than 0.85. The RMSE

401 value for water clouds is smaller than that for ice clouds, suggesting that water cloud optical properties can
402 reproduce global irradiance better than can ice cloud properties. Although not distinctly different, the absolute
403 MBE value is smaller for water clouds than for ice clouds. Overall, these results suggest that retrieval accuracies
404 are better for water cloud properties than for ice cloud properties in SGLI. Note that the COD values from the sky
405 radiometer also agree better for water clouds than for ice clouds. The MBE values are negative for both water and
406 ice clouds, suggesting that the modeled global irradiances are generally higher than the observed values. Such
407 negative MBE values (overestimation of modeled global irradiances) can result from underestimated COD values
408 in SGLI. This result again coincides with the positive MBE values for the comparisons of COD between the sky
409 radiometer and SGLI shown in Figure 1. Furthermore, Figure 12 shows scatter plots for the normalized differences
410 between the modeled and measured values and the observed values. The observed global irradiance can suggest
411 the COD, with a low global irradiance corresponding to a high COD and vice versa. Figure 12 suggests
412 overestimated values of the modeled global irradiance when the observed values are relatively low, suggesting
413 underestimated COD in SGLI when the clouds are optically thick. This result again coincides with the comparison
414 of COD between the sky radiometer and SGLI shown in Figure 1 and discussed in section 4.1.1. The fewer data
415 samples for water clouds hardly suggest underestimated modeled irradiance (overestimated SGLI COD) when the
416 observed global irradiance is relatively high, but it is somewhat evident in ice clouds. This result again supports
417 the underestimation (resp. overestimation) of COD from SGLI when the clouds are relatively thick (resp. thin), as
418 discussed in section 4.1.1.

419 Unlike the COD comparisons shown for different cloud types and SZA and VZA values, the measured and
420 modeled global irradiances do not show distinct differences depending on cloud type and SZA and VZA values.
421 This is likely due to the fact that the global-irradiance-observing pyranometer has a wide FOV. Khatri et al. (2019)
422 discussed the importance of an instrument's FOV for cloud remote sensing.

423

424 5. Conclusions

425 The main findings of this study are summarized below.

- 426 1. The COD values from SGLI agreed reasonably well with the values observed from the surface using a sky
427 radiometer by showing correlation coefficient (r) values of ~ 0.8 and ~ 0.6 , RMSE values of ~ 10 and ~ 8 , and
428 MBE values of ~ 3 and ~ 3 for water and ice clouds, respectively. There appears to be a tendency of
429 underestimating (resp. overestimating) the COD in SGLI for relatively thick (resp. thin) clouds. By contrast,
430 the CER comparisons showed poorer agreements than the COD values, with r values of ~ 0.1 and ~ 0.3 , RMSE
431 values of ~ 7 and $\sim 18 \mu\text{m}$, and MBE values of ~ -0.5 and $\sim -10 \mu\text{m}$ for water and ice clouds, respectively.
- 432 2. Comparison analyses performed by separating cloud types revealed that relatively thin, possibly mixed, and
433 horizontally inhomogeneous cloud types generally have larger discrepancies than do relatively uniform and
434 flat types of clouds for both the water and ice phases of clouds.
- 435 3. The COD differences between SGLI and the sky radiometer showed strong and weak dependencies on SZA
436 for water and ice clouds, respectively, by showing increasing difference with increasing SZA. On the other

437 hand, only the COD difference for water clouds showed a weak dependency on VZA, with increased
438 difference for high VZA.

439 4. Analyses of the SGLI-observed reflection as functions of SZA, VZA, and COD and similar values of
440 computed reflection functions by using a 1D radiative-transfer model (assuming PPH cloud layers) were
441 inconsistent with each other, indicating that the 1D model was insufficient for capturing 3D cloud effects on
442 the observed signals and thereby SZA and VZA biases on the retrieved cloud properties.

443 5. The surface global irradiances calculated using the SGLI-observed cloud properties agreed very well with
444 the surfaced-observed values, with r values of ~ 0.9 and ~ 0.9 , RMSE values of ~ 66 and $\sim 91 \text{ Wm}^{-2}$, and MBE
445 values of ~ -32 and $\sim -33 \text{ Wm}^{-2}$ for water and ice clouds, respectively. These results further revealed higher
446 values of modeled irradiances than observed values when the latter were relatively low, and vice versa. These
447 results further justified the evaluations of SGLI COD performed using the sky radiometer by emphasizing
448 that (i) the SGLI COD can be underestimated on average, (ii) water cloud properties may have better retrieval
449 accuracies than do ice cloud properties, and (iii) the SGLI COD can be underestimated (resp. overestimated)
450 for optically thick (resp. thin) clouds.

451

452 *Code availability.* Codes for data analyses are available from the corresponding author upon request.

453

454 *Data availability.* SGLI data can be downloaded from Global Portal System (G-portal) of JAXA
455 (<https://gportal.jaxa.jp/gpr/>). Similarly, global irradiance data can be downloaded from SKYNET webpage
456 (<http://atmos3.cr.chiba-u.jp/skyenet/>). Cloud properties retrieved from sky radiometer observations can be obtained
457 from the corresponding author upon request.

458

459 *Author contributions.* PK and TH developed the study framework. HI and TT generated data. PK, HL, TN, and HI
460 developed algorithms.

461

462 *Competing interests.* The authors declare that they have no conflict of interest.

463

464 *Special issue statement.* This article is part of the special issue “SKYNET – the international network for aerosol,
465 clouds, and so-lar radiation studies and their applications (AMT/ACP inter-journal SI)”. It is not associated with
466 a conference.

467

468 *Acknowledgements:* This research is supported by the 2nd Research Announcement on the Earth Observations of
469 the Japan Aerospace Exploration Agency (JAXA) (PI No. ER2GCF211, Contract No. 19RT000370), a Grant-in-
470 Aid for Scientific Research (C) 17K05650 from Japan Society for the Promotion of Science (JSPS), and “Virtual
471 Laboratory for Diagnosing the Earth’s Climate System” program of MEXT, Japan.

472

473 **References**

474 Cahalan, R. F., Ridgway, W., Wiscombe, W. J., Bell, T. L. and Snider, J. B.: The albedo of fractal stratocumulus
475 clouds, *Journal of the Atmospheric Sciences*, 51, 2434-2455,10.1175/1520-
476 0469(1994)051<2434:TAOFSC>2.0.CO;2, 1994.

477 Campanelli, M., Nakajima, T., Khatri, P., Takamura, T., Uchiyama, A., Estelles, V., Liberti, G. L., and Malvestuto,
478 V.: Retrieval of characteristic parameters for water vapour transmittance in the development of ground-based
479 sun-sky radiometric measurements of columnar water vapour, *Atmospheric Measurement Techniques*, 7,
480 1075-1087, 10.5194/amt-7-1075-2014, 2014.

481 Cess, R. D., Zhang, M. H., Zhou, Y., Jing, X., and Dvortsov, V.: Absorption of solar radiation by clouds:
482 Interpretations of satellite, surface, and aircraft measurements, *Journal of Geophysical Research: Atmospheres*,
483 101, 23299-23309, 10.1029/96jd02156, 1996.

484 Chiu, J. C., Marshak, A., Huang, C. H., Várnai, T., Hogan, R. J., Giles, D. M., Holben, B. N., O'Connor, E. J.,
485 Knyazikhin, Y., and Wiscombe, W. J.: Cloud droplet size and liquid water path retrievals from zenith radiance
486 measurements: examples from the Atmospheric Radiation Measurement Program and the Aerosol Robotic
487 Network, *Atmospheric Chemistry and Physics*, 12, 10313-10329, 10.5194/acp-12-10313-2012, 2012.

488 Damiani, A., Irie, H., Horio, T., Takamura, T., Khatri, P., Takenaka, H., Nagao, T., Nakajima, T. Y., and Cordero,
489 R. R.: Evaluation of Himawari-8 surface downwelling solar radiation by ground-based measurements,
490 *Atmospheric Measurement Techniques*, 11, 2501-2521, 10.5194/amt-11-2501-2018, 2018.

491 Damiani, A., Irie, H., Takamura, T., Kudo, R., Khatri, P., Iwabuchi, H., Masuda, R., and Nagao, T.: An Intensive
492 Campaign-Based Intercomparison of Cloud Optical Depth from Ground and Satellite Instruments under
493 Overcast Conditions, *Sola*, 15, 198-204, 10.2151/sola.2019-036, 2019.

494 Dong, X., Minnis, P., Xi, B., Sun-Mack, S., and Chen, Y.: Comparison of CERES-MODIS stratus cloud properties
495 with ground-based measurements at the DOE ARM Southern Great Plains site, *Journal of Geophysical
496 Research*, 113, 10.1029/2007jd008438, 2008.

497 Forster, P., T. Storelvmo, K. Armour, W. Collins, J.-L. Dufresne, D. Frame, D.J. Lunt, T. Mauritsen, M.D. Palmer,
498 M. Watanabe, M. Wild, and H. Zhang: The Earth's Energy Budget, Climate Feedbacks, and Climate Sensitivity.
499 In *Climate Change 2021: The Physical Science Basis. Contribution of Working Group I to the Sixth
500 Assessment Report of the Intergovernmental Panel on Climate Change* [Masson-Delmotte, V., P. Zhai, A.
501 Pirani, S.L. Connors, C. Péan, S. Berger, N. Caud, Y. Chen, L. Goldfarb, M.I. Gomis, M. Huang, K. Leitzell,
502 E. Lonnoy, J.B.R. Matthews, T.K. Maycock, T. Waterfield, O. Yelekçi, R. Yu, and B. Zhou (eds.)]. Cambridge
503 University Press. In Press., 2021.

504 Fu, Q., Cribb, M. C., Barker, H. W., Krueger, S. K., and Grossman A.: Cloud geometry effects on atmospheric
505 solar absorption, *Journal of the Atmospheric Sciences*, 57, 1156-1168, doi:10.1175/1520-
506 0469(2000)057<1156:CGEOAS>2.0.CO;2, 2000.

507 Hashimoto, M., Nakajima, T., Dubovik, O., Campanelli, M., Che, H., Khatri, P., Takamura, T., and Pandithurai,
508 G.: Development of a new data-processing method for SKYNET sky radiometer observations, *Atmospheric
509 Measurement Techniques*, 5, 2723-2737, 10.5194/amt-5-2723-2012, 2012.

510 IPCC: Climate Change 2021: The Physical Science Basis. Contribution of Working Group I to the Sixth
511 Assessment Report of the Intergovernmental Panel on Climate Change [Masson-Delmotte, V., P. Zhai, A.
512 Pirani, S.L. Connors, C. Péan, S. Berger, N. Caud, Y. Chen, L. Goldfarb, M.I. Gomis, M. Huang, K. Leitzell,
513 E. Lonnoy, J.B.R. Matthews, T.K. Maycock, T. Waterfield, O. Yelekçi, R. Yu, and B. Zhou (eds.)]. Cambridge
514 University Press. In Press., 2021.

515 Irie, H., Hoque, H. M. S., Damiani, A., Okamoto, H., Fatmi, A. M., Khatri, P., Takamura, T., and Jarupongsakul,
516 T.: Simultaneous observations by sky radiometer and MAX-DOAS for characterization of biomass burning
517 plumes in central Thailand in January–April 2016, *Atmospheric Measurement Techniques*, 12, 599-606,
518 10.5194/amt-12-599-2019, 2019.

519 Ishimoto, H., Masuda, K., Mano, Y., Orikasa, N., and Uchiyama, A.: Irregularly shaped ice aggregates in optical
520 modeling of convectively generated ice clouds, *Journal of Quantitative Spectroscopy and Radiative Transfer*,
521 113, 632-643, 10.1016/j.jqsrt.2012.01.017, 2012.

522 Iwabuchi, H., and Tadahiro, H.: Effects of Cloud Horizontal Inhomogeneity on the Optical Thickness Retrieved
523 from Moderate-Resolution Satellite Data, *Journal of the Atmospheric Sciences*, 59, 2227–2242,
524 [https://doi.org/10.1175/1520-0469\(2002\)059<2227:EOCHIO>2.0.CO;2](https://doi.org/10.1175/1520-0469(2002)059<2227:EOCHIO>2.0.CO;2), 2002.

525 Kato, S., Hinkelman, L. M., and Cheng, A.: Estimate of satellite-derived cloud optical thickness and effective
526 radius errors and their effect on computed domain-averaged irradiances, *Journal of Geophysical Research*, 111,
527 10.1029/2005jd006668, 2006.

528 Kato, S. and Marshak, A.: Solar zenith and viewing geometry-dependent errors in satellite retrieved cloud optical
529 thickness: Marine stratocumulus case, *Journal of Geophysical Research: Atmospheres*, 114,
530 10.1029/2008jd010579, 2009.

531 Kawamoto, K., Nakajima, T., and Nakajima, T. Y.: A Global Determination of Cloud Microphysics with AVHRR
532 Remote Sensing, *Journal of Climate*, 14, 4043–4059, [https://doi.org/10.1175/1520-
533 0469\(1995\)052<4043:WADOCM>2.0.CO;2](https://doi.org/10.1175/1520-0469(1995)052<4043:WADOCM>2.0.CO;2), 2000.

534 Khatri, P., Hayasaka, T., Holben, B., Tripathi, S. N., Misra, P., Patra, P. K., Hayashida, S., and Dumka, U. C.:
535 Aerosol Loading and Radiation Budget Perturbations in Densely Populated and Highly Polluted Indo-Gangetic
536 Plain by COVID-19: Influences on Cloud Properties and Air Temperature, *Geophysical Research Letters*, 48,
537 10.1029/2021gl093796, 2021.

538 Khatri, P., Hayasaka, T., Iwabuchi, H., Takamura, T., Irie, H., and Nakajima, T. Y.: Validation of MODIS and
539 AHI Observed Water Cloud Properties Using Surface Radiation Data, *Journal of the Meteorological Society
540 of Japan. Ser. II*, 96B, 151-172, 10.2151/jmsj.2018-036, 2018b.

541 Khatri, P., Iwabuchi, H., Hayasaka, T., Irie, H., Takamura, T., Yamazaki, A., Damiani, A., Letu, H., and Kai, Q.:
542 Retrieval of cloud properties from spectral zenith radiances observed by sky radiometers, *Atmospheric
543 Measurement Techniques*, 12, 6037-6047, 10.5194/amt-12-6037-2019, 2019.

544 Khatri, P., Iwabuchi, H., and Saito, M.: Vertical Profiles of Ice Cloud Microphysical Properties and Their Impacts
545 on Cloud Retrieval Using Thermal Infrared Measurements, *Journal of Geophysical Research: Atmospheres*,
546 123, 5301-5319, 10.1029/2017jd028165, 2018a.

547 Khatri, P., Ooashi, H., and Iwabuchi, H.: Investigating Aerosol Effects on Maritime Deep Convective Clouds
548 Using Satellite and Reanalysis Data, *Sola*, 16, 228-232, 10.2151/sola.2020-038, 2020.

549 Khatri, P. and Takamura, T.: An Algorithm to Screen Cloud Affected Data for Sky Radiometer Data Analysis,
550 *Journal of the Meteorological Society of Japan*, 87, 189-204, 10.2151/jmsj.87.189, 2009.

551 Khatri, P., Takamura, T., Shimizu, A., and Sugimoto, N.: Spectral Dependency of Aerosol Light-Absorption over
552 the East China Sea Region, *Sola*, 6, 1-4, 10.2151/sola.2010-001, 2010.

553 Khatri, P., Takamura, T., Shimizu, A., and Sugimoto, N.: Observation of low single scattering albedo of aerosols
554 in the downwind of the East Asian desert and urban areas during the inflow of dust aerosols, *Journal of*
555 *Geophysical Research: Atmospheres*, 119, 787-802, 10.1002/2013jd019961, 2014a.

556 Khatri, P., Tamio, T., Yamazaki, A., and Kondo, Y.: Retrieval of Key Aerosol Optical Parameters from Spectral
557 Direct and Diffuse Irradiances Observed by a Radiometer with Nonideal Cosine Response Characteristic,
558 *Journal of Atmospheric and Oceanic Technology*, 29, 683-696, 10.1175/jtech-d-11-00111.1, 2012.

559 Khatri, P., Takamura, T., Yamazaki, A., and Uchiyama, A.: Use of 315 nm Channel Data of the Sky Radiometer
560 to Estimate the Columnar Ozone Concentration: A Preliminary Study, *Journal of the Meteorological Society*
561 *of Japan. Ser. II*, 92A, 185-194, 10.2151/jmsj.2014-A12, 2014b.

562 Khatri, P., Takamura, T., Nakajima, T., Estellés, V., Irie, H., Kuze, H., Campanelli, M., Sinyuk, A., Lee, S. M.,
563 Sohn, B. J., Pandithurai, G., Kim, S. W., Yoon, S. C., Martinez-Lozano, J. A., Hashimoto, M., Devara, P. C.
564 S., and Manago, N.: Factors for inconsistent aerosol single scattering albedo between SKYNET and
565 AERONET, *Journal of Geophysical Research: Atmospheres*, 121, 1859-1877, 10.1002/2015jd023976, 2016.

566 King, N. J., Bower, K. N., Crosier, J., and Crawford, I.: Evaluating MODIS cloud retrievals with in situ
567 observations from VOCALS-REx, *Atmospheric Chemistry and Physics*, 13, 191-209, 10.5194/acp-13-191-
568 2013, 2013.

569 Letu, H., Nakajima, T. Y., Wang, T., Shang, H., Ma, R., Yang, K., Baran, A. J., Riedi, J., Ishimoto, H., Yoshida,
570 M., Shi, C., Khatri, P., Du, Y., Chen, L., and Shi, J.: A new benchmark for surface radiation products over the
571 East Asia-Pacific region retrieved from the Himawari-8/AHI next-generation geostationary satellite, *Bulletin*
572 *of the American Meteorological Society*, 1-40, 10.1175/bams-d-20-0148.1, 2021.

573 Letu, H., Yang, K., Nakajima, T. Y., Ishimoto, H., Nagao, T. M., Riedi, J., Baran, A. J., Ma, R., Wang, T., Shang,
574 H., Khatri, P., Chen, L., Shi, C., and Shi, J.: High-resolution retrieval of cloud microphysical properties and
575 surface solar radiation using Himawari-8/AHI next-generation geostationary satellite, *Remote Sensing of*
576 *Environment*, 239, 10.1016/j.rse.2019.111583, 2020.

577 Liang, L. and Girolamo, L. D.: A global analysis on the view-angle dependence of plane-parallel oceanic liquid
578 water cloud optical thickness using data synergy from MISR and MODIS, *Journal of Geophysical Research:*
579 *Atmospheres*, 118, 2389-2403, 10.1029/2012jd018201, 2013.

580 Liu, J., Li, Z., Zheng, Y., Chiu, J. C., Zhao, F., Cadetdu, M., Weng, F., and Cribb, M.: Cloud optical and
581 microphysical properties derived from ground-based and satellite sensors over a site in the Yangtze Delta
582 region, *Journal of Geophysical Research: Atmospheres*, 118, 9141-9152, 10.1002/jgrd.50648, 2013.

583 Loeb, N. G., and Coakley, Jr., J. A. : Inference of marine stratus cloud optical depths from satellite measurements:
584 Does 1D theory apply?, *Journal of Climate*, 11, 215–233, doi:10.1175/1520-
585 0442(1998)011 <0215:IOMSCO > 2.0.CO;2, 1998.

586 Loeb, N. G., and Davies, R. : Angular dependence of observed reflectances: A comparison with plane parallel
587 theory, *Journal of Geophysical Research: Atmospheres*, 102, 6865–6881, 10.1029/96JD03586, 1997.

588 Loeb, N. G., Várnai, T., and Davies, R.: Effect of cloud inhomogeneities on the solar zenith angle dependence of
589 nadir reflectance, *Journal of Geophysical Research: Atmospheres*, 102(DD8), 9387–9395,
590 doi:10.1029/96JD03719, 1997.

591 Masunaga, H., Satoh, M., and Miura, H.: A joint satellite and global cloud-resolving model analysis of a Madden-
592 Julian Oscillation event: Model diagnosis, *Journal of Geophysical Research*, 113, 10.1029/2008jd009986, 2008.

593 Mok, J., Krotkov, N. A., Torres, O., Jethva, H., Li, Z., Kim, J., Koo, J.-H., Go, S., Irie, H., Labow, G., Eck, T. F.,
594 Holben, B. N., Herman, J., Loughman, R. P., Spinei, E., Lee, S. S., Khatri, P., and Campanelli, M.:
595 Comparisons of spectral aerosol single scattering albedo in Seoul, South Korea, *Atmospheric Measurement*
596 *Techniques*, 11, 2295–2311, 10.5194/amt-11-2295-2018, 2018.

597 Nakajima, T., Campanelli, M., Che, H., Estellés, V., Irie, H., Kim, S.-W., Kim, J., Liu, D., Nishizawa, T.,
598 Pandithurai, G., Soni, V. K., Thanu, B., Tugjurn, N.-U., Aoki, K., Go, S., Hashimoto, M., Higurashi, A.,
599 Kazadzis, S., Khatri, P., Kouremeti, N., Kudo, R., Marengo, F., Momoi, M., Ningombam, S. S., Ryder, C. L.,
600 Uchiyama, A., and Yamazaki, A.: An overview of and issues with sky radiometer technology and SKYNET,
601 *Atmospheric Measurement Techniques*, 13, 4195–4218, 10.5194/amt-13-4195-2020, 2020.

602 Nakajima, T. and King, M. D.: Determination of the Optical Thickness and Effective Particle Radius of Clouds
603 from Reflected Solar Radiation Measurements. Part I: Theory, *Journal of the Atmospheric Sciences*, 47, 1878–
604 1893, [https://doi.org/10.1175/1520-0469\(1990\)047<1878:DOTOTA>2.0.CO;2](https://doi.org/10.1175/1520-0469(1990)047<1878:DOTOTA>2.0.CO;2), 1990.

605 Nakajima, T., King, M. D., Spinfire, J. D., and Radke, L. F.: Determination of the Optical Thickness and Effective
606 Particle Radius of Clouds from Reflected Solar Radiation Measurements. Part II: Marine Stratocumulus
607 Observations, *Journal of the Atmospheric Sciences*, 48, 728–751, [https://doi.org/10.1175/1520-0469\(1991\)048<0728:DOTOTA>2.0.CO;2](https://doi.org/10.1175/1520-0469(1991)048<0728:DOTOTA>2.0.CO;2), 1991.

609 Nakajima, T., and Tanaka M.: Matrix formulation for the transfer of solar radiation in a plane-parallel scattering
610 atmosphere, *Journal of Quantitative Spectroscopy & Radiative Transfer*, 35, 13–21, 10.1016/0022-
611 4073(86)90088-9, 1986.

612 Nakajima, T., and Tanaka M.: Algorithms for radiative intensity calculations in moderately thick atmospheres
613 using a truncation approximation, *Journal of Quantitative Spectroscopy & Radiative Transfer*, 40, 51–69,
614 10.1016/0022-4073(88)90031-3, 1988.

615 Nakajima, T. Y., Ishida, H., Nagao, T. M., Hori, M., Letu, H., Higuchi, R., Tamaru, N., Imoto, N., and Yamazaki,
616 A.: Theoretical basis of the algorithms and early phase results of the GCOM-C (Shikisai) SGLI cloud products,
617 *Progress in Earth and Planetary Science*, 6, 10.1186/s40645-019-0295-9, 2019.

618 Nakajima, T. Y. and Nakajima, T.: Wide-Area Determination of Cloud Microphysical Properties from NOAA
619 AVHRR Measurements for FIRE and ASTEX Regions, *Journal of Atmospheric Sciences*, 52, 4043–4059,
620 [https://doi.org/10.1175/1520-0469\(1995\)052<4043:WADOCM>2.0.CO;2](https://doi.org/10.1175/1520-0469(1995)052<4043:WADOCM>2.0.CO;2), 1995.

621 Painemal, D. and Zuidema, P.: Assessment of MODIS cloud effective radius and optical thickness retrievals over
622 the Southeast Pacific with VOCALS-REx in situ measurements, *Journal of Geophysical Research:*
623 *Atmospheres*, 116, n/a-n/a, 10.1029/2011jd016155, 2011.

624 Ramanathan, V., Cess, R. D., Harrison, E. F., Minnis, P., Barkstrom, B. R., Ahmad, E., and Hartmann, D.: Cloud-
625 radiative forcing and climate: results from the Earth radiation budget experiment, *Science*, 243, 57-63,
626 10.1126/science.243.4887.57, 1989.

627 Rodgers, C. D.: *Inverse Methods for Atmospheric Sounding: Theory and Practice (Vol. 2)*, Ser. Atmos. Oceanic
628 Planet. Phys., 2, World Sci., Hackensack, NJ, 2000.

629 Rosenfeld, D., Andreae, M. O., Asmi, A., Chin, M., de Leeuw, G., Donovan, D. P., Kahn, R., Kinne, S., Kivekäs,
630 N., Kulmala, M., Lau, W., Schmidt, K. S., Suni, T., Wagner, T., Wild, M., and Quaas, J.: Global observations
631 of aerosol-cloud-precipitation-climate interactions, *Reviews of Geophysics*, 52, 750-808,
632 10.1002/2013rg000441, 2014.

633 Takamura, T. and Khatri, P.: Uncertainties in Radiation Measurement Using a Rotating Shadow-Band
634 Spectroradiometer, *Journal of the Meteorological Society of Japan. Ser. II*, 99, 1547-1561, 10.2151/jmsj.2021-
635 075, 2021.

636 Várnai, T. and Marshak, A.: View angle dependence of cloud optical thicknesses retrieved by Moderate Resolution
637 Imaging Spectroradiometer (MODIS), *Journal of Geophysical Research*, 112, 10.1029/2005jd006912, 2007.

638 Wang, Z., Liu, D., Wang, Z., Wang, Y., Khatri, P., Zhou, J., Takamura, T., and Shi, G.: Seasonal characteristics
639 of aerosol optical properties at the SKYNET Hefei site (31.90°N, 117.17°E) from 2007 to 2013, *Journal of*
640 *Geophysical Research: Atmospheres*, 119, 6128-6139, 10.1002/2014jd021500, 2014.

641 Yan, H., Huang, J., Minnis, P., Yi, Y., Sun-Mack, S., Wang, T., and Nakajima, T. Y.: Comparison of CERES-
642 MODIS cloud microphysical properties with surface observations over Loess Plateau, *Journal of Quantitative*
643 *Spectroscopy and Radiative Transfer*, 153, 65-76, 10.1016/j.jqsrt.2014.09.009, 2015.

644 Zhang, Z. and Platnick, S.: An assessment of differences between cloud effective particle radius retrievals for
645 marine water clouds from three MODIS spectral bands, *Journal of Geophysical Research*, 116,
646 10.1029/2011jd016216, 2011.

647
648
649
650
651
652
653
654

655

656

657

658 Table 1. SKYNET sites for surface observation data

Location	Longitude (°E)	Latitude (°N)
Chiba	140.104	35.625
Hedo-misaki	128.248	26.867
Fukue-jima	128.682	32.752
Miyako-jima*	125.327	24.737
Sendai	140.839	38.259

659 *Missing of surface radiative flux data

660

661 Table 2. Mean values of SZA and VZA for different levels of differences in water cloud properties observed by
662 sky radiometer and SGLI

Diff. Range	COD			CER		
	SZA(°)	VZA(°)	N	SZA(°)	VZA(°)	N
0-30%	35.76±11.42	25.66±15.20	43	37.35±12.59	27.07±14.07	34
30-60%	38.41±8.44	23.68±16.83	13	36.99±10.11	26.90±16.72	20
60-90%	48.52±9.37	29.77±12.53	5	42.70±10.38	25.32±11.26	4
> 90%	53.10±2.84	29.05±5.28	3	43.03±7.16	14.58±12.80	6

663

664

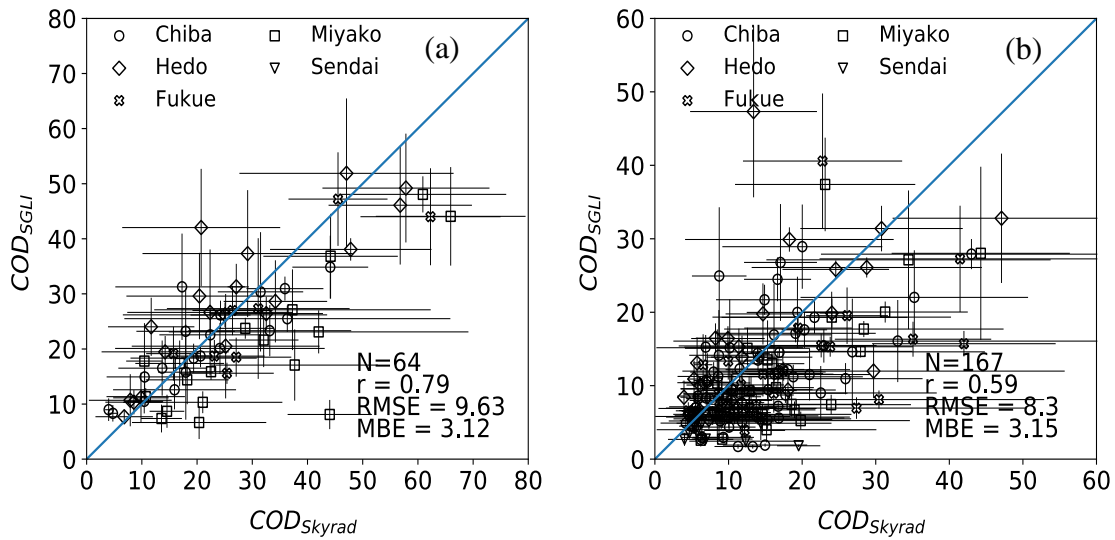
665 Table 3. Mean values of SZA and VZA for different levels of differences in ice cloud properties observed by sky
666 radiometer and SGLI

Diff. Range	COD			CER		
	SZA(°)	VZA(°)	N	SZA(°)	VZA(°)	N
0-30%	33.62±12.67	26.96±12.67	63	31.29±12.51	25.97±14.27	53
30-60%	32.09±12.65	27.60±14.46	72	33.62±13.27	27.63±12.32	30
60-90%	33.75±12.22	25.89±13.52	29	32.95±13.98	27.31±12.19	25
> 90%	44.20±12.25	26.08±13.96	9	36.62±12.34	27.85±14.02	52

667

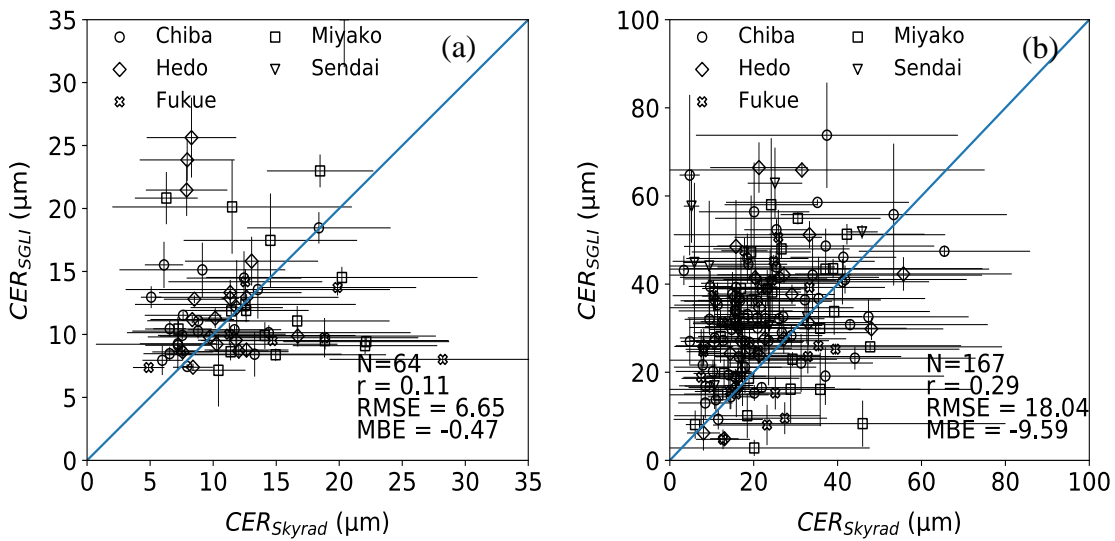
668

669



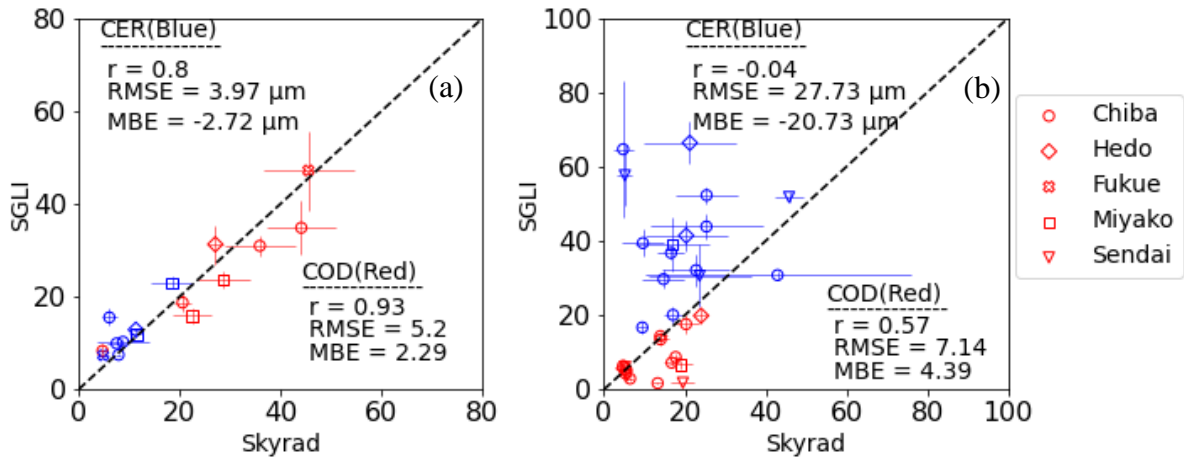
670
 671
 672
 673
 674
 675

Figure 1. Comparison of COD between sky radiometer and SGLI for (a) water clouds and (b) ice clouds for data collected over SKYNET sites.



676
 677
 678
 679
 680
 681

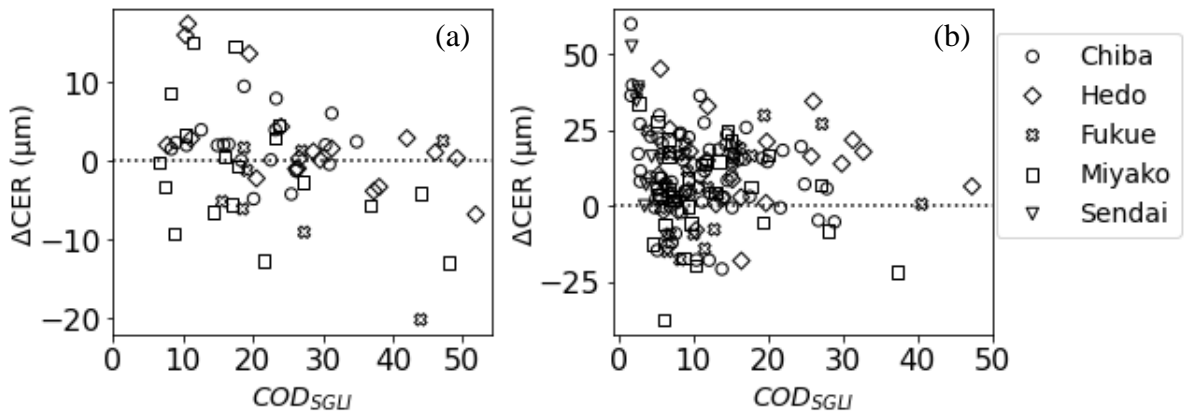
Figure 2. As Figure 1 but for CER.



682

683 **Figure 3. Comparison of cloud properties (COD and CER) between sky radiometer and SGLI for (a) water**
 684 **clouds and (b) ice clouds by selecting data samples with coefficient of variation (COV) less than 0.2.**

685



686

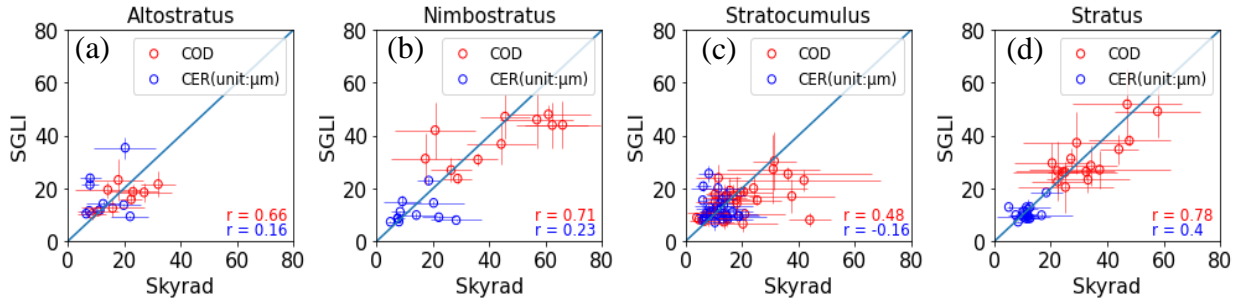
687 **Figure 4. Comparison between Δ CER ($CER_{SGLI} - CER_{skyrad}$) and $SGLI_{COD}$ for (a) water clouds and (b) ice**
 688 **clouds.**

689

690

691

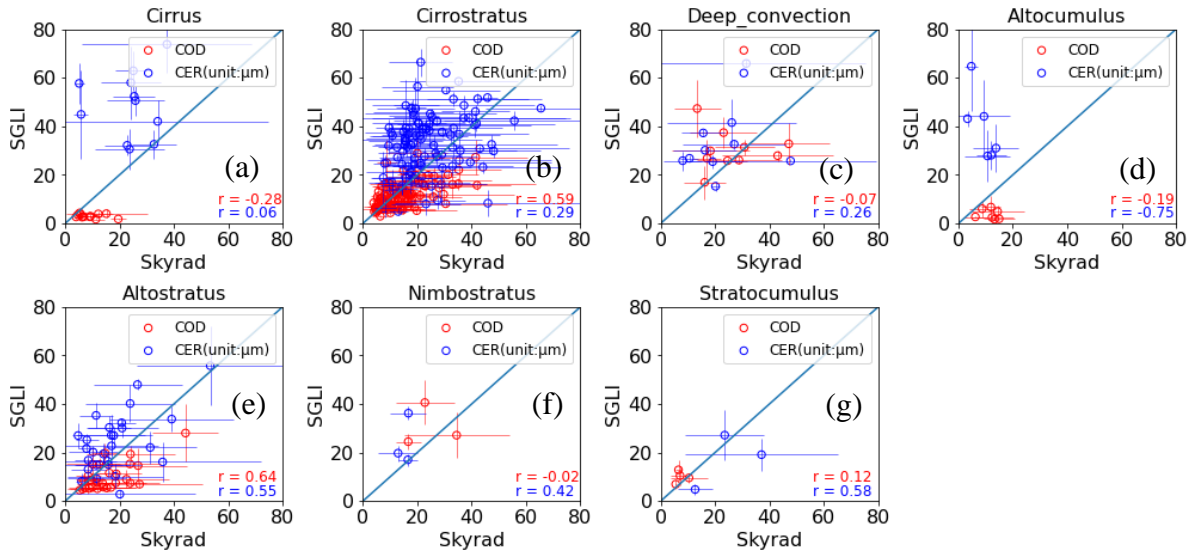
692



693

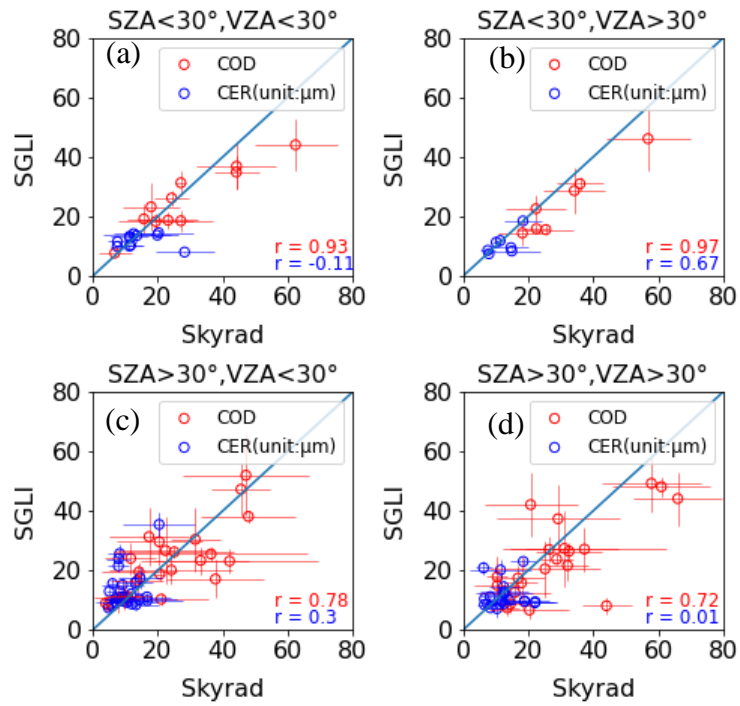
694 **Figure 5. Comparison between sky radiometer-observed and SGLI-observed water cloud properties for**
 695 **different types of clouds. The cloud type corresponds to the central pixel of 5x5 SGLI pixels.**

696



697

698 **Figure 6. As Figure 3 but for ice cloud properties.**

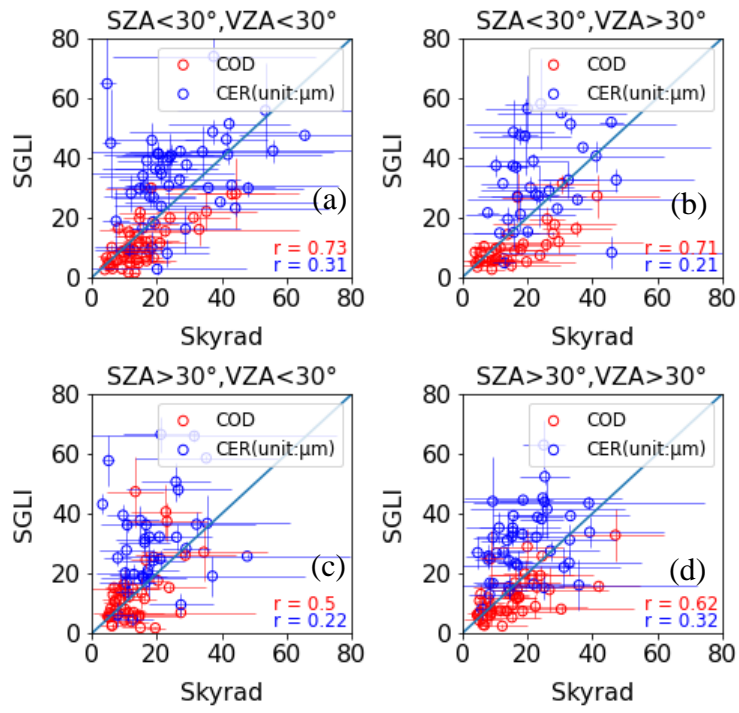


699

700 **Figure 7. Comparison between sky radiometer-observed and SGLI-observed water cloud properties for**
 701 **each SZA and VZA greater than and less than 30°. The SZA and VZA values correspond to the central**
 702 **pixel of 5x5 SGLI pixels.**

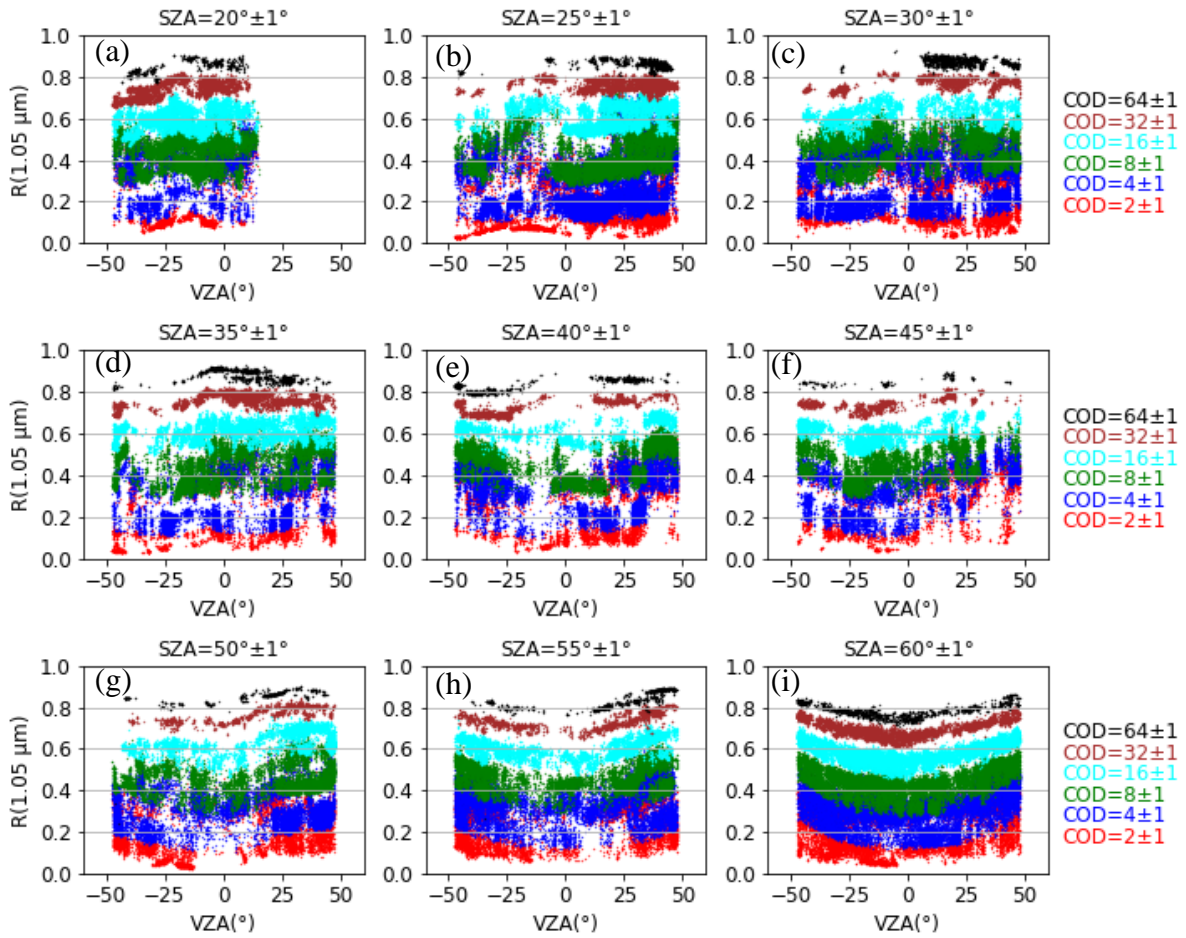
703

704



705

706 **Figure 8.** As Figure 5 but for ice cloud properties.



707

708 **Figure 9. Scatter plots of observed $R(1.05 \mu\text{m})$ – VZA relationships for different COD values of water clouds**
 709 **at different SZA values. The data are for 500 pixels centered on the Chiba observation site in 2020. The**
 710 **negative and positive VZA values represent the forward ($RAZ > 90^\circ$) and backward ($RAZ < 90^\circ$) scattering**
 711 **directions, respectively.**

712

713

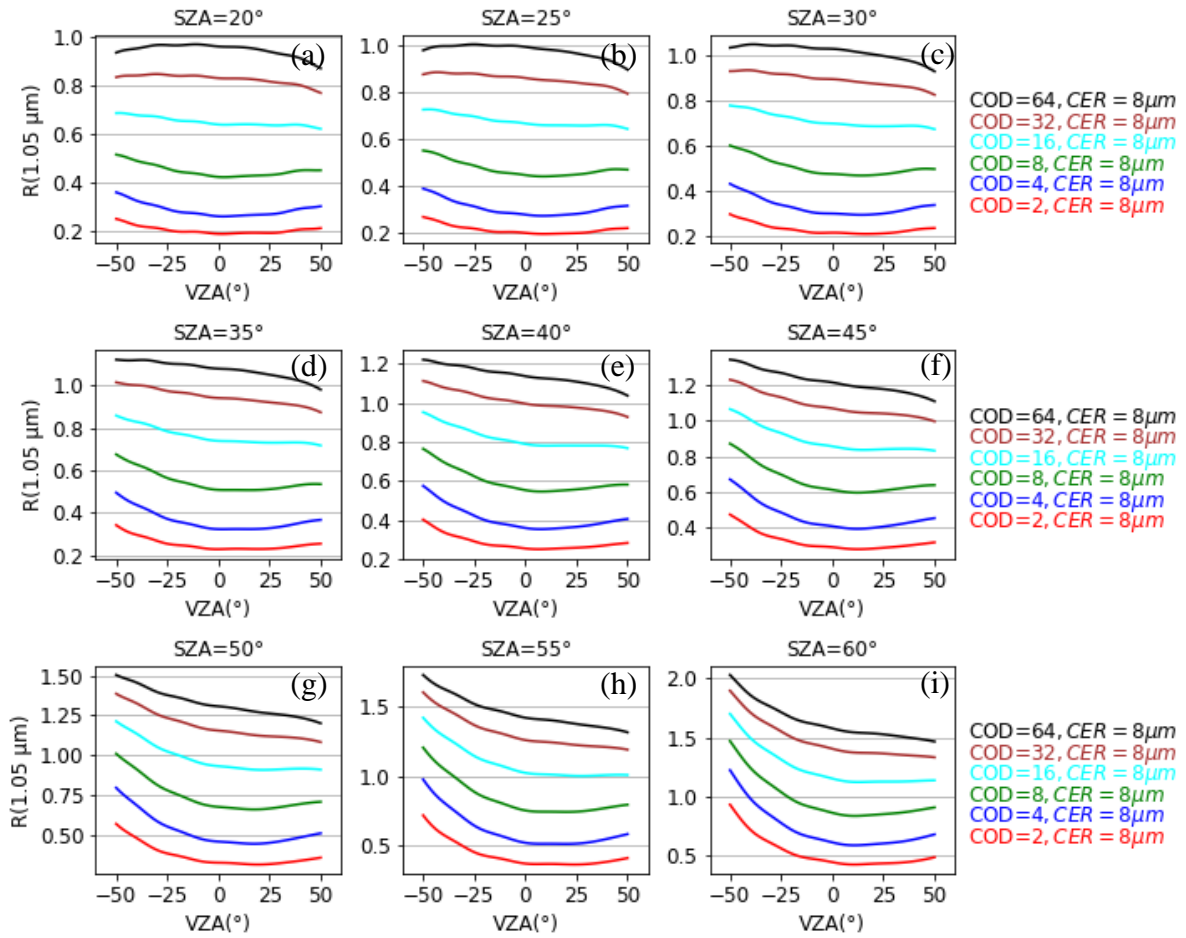
714

715

716

717

718



719

720 **Figure 10. Relationship between $R(1.05 \mu\text{m})$ and VZA for different COD values and fixed CER of $8 \mu\text{m}$ for**
 721 **water clouds and different SZA values for assumption of plane-parallel cloud layers. The negative and**
 722 **positive VZA values correspond to RAZ values of 135° and 45° representing the forward and backward**
 723 **scattering directions, respectively.**

724

725

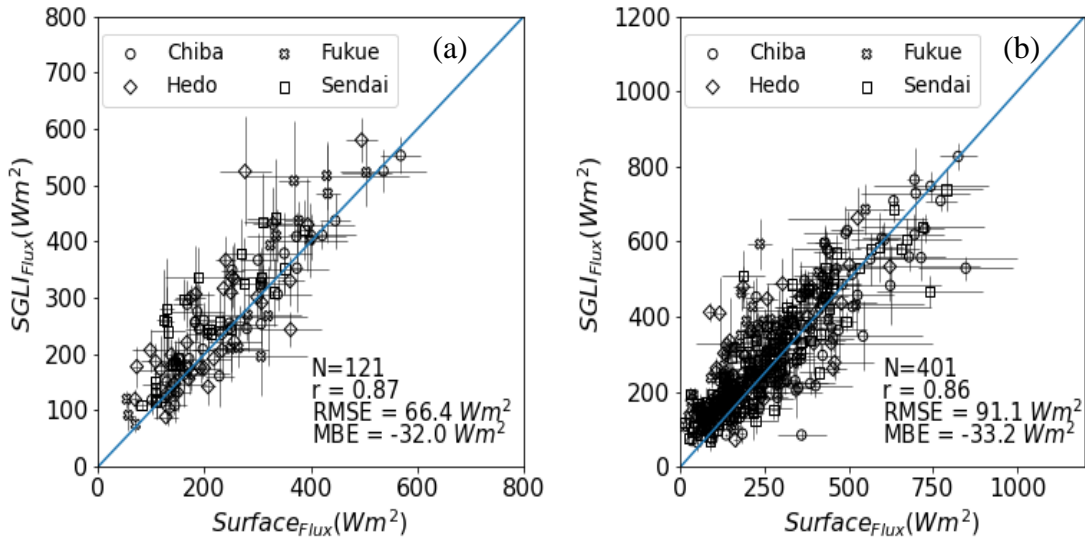
726

727

728

729

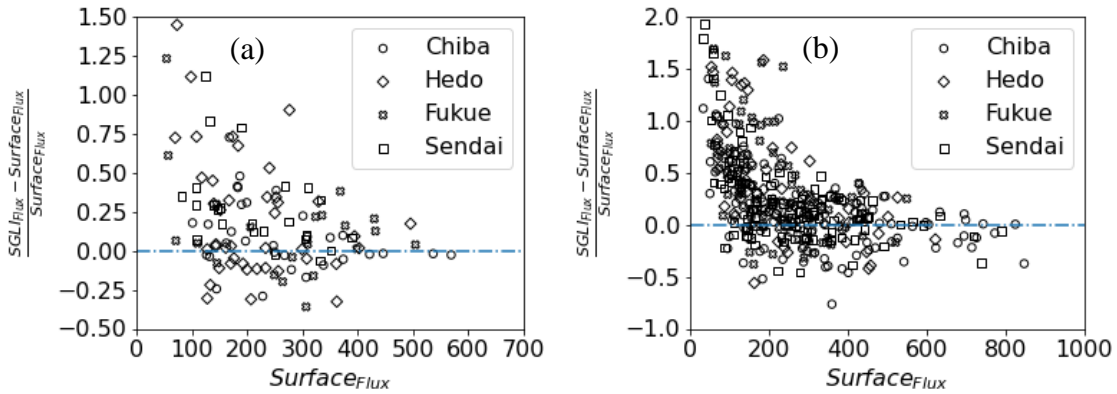
730



731

732 **Figure 11. Comparison of surface-observed global irradiances with values modeled using SGLI-observed**
 733 **cloud properties for (a) water clouds and (b) ice clouds.**

734



735

736 **Figure 12. Scatter plots for modeled and observed global-irradiance difference and observed global**
 737 **irradiance for (a) water clouds and (b) ice clouds.**